INT. J. NUM. METHODS HEAT FLUID FLOW, VOL. 1, 31–49 (1991)

MIXED LAMINAR HEAT AND FLUID FLOW IN FLOW-THROUGH OPENED TRAPEZOIDAL COOLING CHAMBERS OF LOW ASPECT RATIOS

T. S. LEE

Department of Mechanical and Production Engineering, National University of Singapore, Singapore 0511, Singapore

ABSTRACT

Heat and fluid flow through a trapezoidal cooling chamber were studied numerically. Hot fluid is assumed inflow at some depth below the surface into one end of the chamber and withdrawn at another depth from the other end. The top of the chamber is exposed to the surrounding for cooling and the remaining side-walls are all insulated. Inflow Reynolds number R_o considered is in the range of 100 to 1000 and the inlet densimetric Froude number F_o considered is in the range of 0.5 to 50.0. Numerical experiments show that the flow and temperature fields in the flow-through trapezoidal chamber are strong function of both F_o and R_o. The submergence ratio D/d_o, chamber length to depth ratio L/D and chamber wall angles are also significant in influencing the flow fields. Comparisons were also made with available experimental and prototype data.

KEY WORDS Cooling chamber Fluid flow Temperature fields

NOMENCLATURE

A	Aspect ratio, $A=(L/D)$
d_e	Diameter of the exit opening of the chamber
d_o	Diameter of inlet opening of the chamber
D	Depth of chamber
D_o	Depth of submergence of inlet opening
D_e	Depth of submergence of exit opening
F_o	Densimetric Froude number, $F_o=V_o/\{gd_o(\rho-\rho_o)/\rho_o\}^{0.5}$
g	Gravitational constant
L	Length of chamber
L_c	Characteristic length, $L_c=(L\times D)^{1/2}$
M, N	Mesh sizes
Pr	Prandtl number, $Pr=\nu/\alpha$
P	Pressure
R_a	Rayleigh number, $R_a=\beta gL^3\nabla T/\nu\alpha$
R_o	Reynolds number $R_o=V_od_o/\nu$
Δt	Time increment
T	Temperature
T_a	Temperature of ambient air
T_o	Temperature of inlet hot fluid
T_e	Equilibrium liquid surface temperature
u	Velocity in the x-direction

0961–5539/91/010031–19$2.00

Received December 1990

v Velocity in the y-direction
x, y, z Rectangular coordinates
∇^2 Laplace operator
α Thermal diffusivity
β Coefficient of volumetric expansion
ξ Dimensionless transformed x-coordinate
η Dimensionless transformed y-coordinate
θ Dimensionless temperature
ϕ_1, ϕ_2 Angles of slope of chamber side walls
ν Kinematic viscosity
ρ_o Reference density
ψ Stream function
ζ Vorticity

INTRODUCTION

The rejection of heat from a body of fluid have been the subject of many research due to their important practical applications in the problems of thermal discharge from power stations[1–27] and the cooling of a confined environment by forced or natural fluid convections[28–45] etc. The patterns of fluid flow within a body of fluid in a confined environment very often determine the efficiency and the mode of heat rejection and/or the quality of the returned fluid to the environment. As a consequence, it is often desirable to be able to understand the fluid motion in a cooling chamber, and to predict, as accurately as possible, whether the heat load from a heat source could be dissipated efficiently out of a given body of cooling fluid under certain flow conditions and limitations.

An example of the numerical experiments on thermal discharge problem was obtained by Barry and Hoffman[1]. An explicit numerical scheme was used to compute the temperature and velocity profiles in a receiving water body. Buoyancy and the equation of motion in the vertical direction were neglected. The solution is valid for very shallow bodies of water. In another numerical experiment, Boericke and Hall[2] analysed the behaviour of the hydraulic and thermal dispersion of heated water discharged into an irregular estuary. The model is based on the shallow water approximation to the momentum equations in two dimensions. The vertical variations in velocity and temperature were neglected. There are various other numerical and experimental studies of thermal discharge problems[3–22], but very few considered the variations of temperature and velocity fields in the vertical plane. This vertical variation of temperature and velocity profiles are important in the study of the cooling chamber problem with low aspect ratio of the chamber ($L/D \leqslant 10$). One such relevant study was performed by Stefan[21–23] in the modelling of spread of heated water over lake. A vertical trapezoidal section of the lake was modelled. The fluid dynamic and temperature fields in the lake were numerically simulated by means of a finite difference procedure. The flow in the reservoir is assumed to be two dimensional in a vertical plane. Inflow is allowed at the surface on one end of the reservoir and outflow occurs at the opposite end. The reservoir inflow is set at a given temperature and velocity so as to simulate the thermal discharge from a power generating facility. Other related studies include the natural and forced convection studies in enclosures[28–45], such as the forced convective cooling of the printed circuit borad in a confined space by Davalath and Bayazitoglu[32]; the numerical experiments of inflow into air-conditioned rooms in a vertical plane by Nielsen[38]. A study of the laminar velocity and temperature fields in a rectangular flow-through reservoir was done by Oberkampf and Crow[39]. Related studies of convective heat and fluid flow in enclosures of various shapes were studied by various investigators recently[34–37]. In the study of inflow into an air-conditioned room, for example, instead of hot fluid being discharged into an enclosed environment, cooled air is introduced into a room.

THE MODEL AND THE GOVERNING EQUATIONS

The model analysed (*Figure 1*) consists of a two-dimensional trapezoidal region, described by its length (L), depth (D) and wall angles (ϕ_1, ϕ_2) at each side of the chamber. The inlet of warm fluid and outlet for cooling fluid are specified at some depths D_o and D_e respectively below the free surface. Similarly, d_o and d_e specify the diameters of the inlet and outlet of the cooling chamber. Heat is convected into the reservoir at the inlet, and is lost through the surface and by convection at the outlet. All the other walls are assumed adiabatic. In the analysis of the flow-through cooling chamber, the following assumptions were also made: (a) flow in the chamber has reached a steady state; (b) temperature variations in the chamber are sufficiently small that Boussinesq approximation is valid; (c) internal energy generation is absent; (d) the heat capacity of the fluid is sufficiently large that the temperature of the fluid is negligibly affected by friction; (e) free surface elevation remains constant.

Define the dimensionless variables: $x^*=x/X$, $y^*=y/Y$, $\theta=(T-T_{ref})/(T-T_{ref})$, $\tilde{u}^*=\tilde{u}/V_o$, $\tilde{\psi}^*=\tilde{\psi}/(V_o d_o)$, $\tilde{\zeta}^*=\tilde{\zeta}/(V_o/d_o)$. X, Y are scaling factors for the x- and y-coordinates respectively and T_{ref} is a reference temperature. The dimensionless governing equations describing the laminar fluid motion in the chamber are:

$$\frac{\partial \tilde{\zeta}^*}{\partial t^*} + \nabla^* \times (\tilde{\zeta}^* \times \tilde{u}^*) = \frac{1}{R_o} \nabla^{*2} \tilde{\zeta}^* - \frac{1}{F_o^2} (\nabla^* \times \theta \hat{g}^*) \tag{1}$$

$$\frac{\partial \theta}{\partial t^*} + \nabla^* \cdot (\tilde{u}\theta) = \frac{1}{R_o Pr} \nabla^{*2} \theta \tag{2}$$

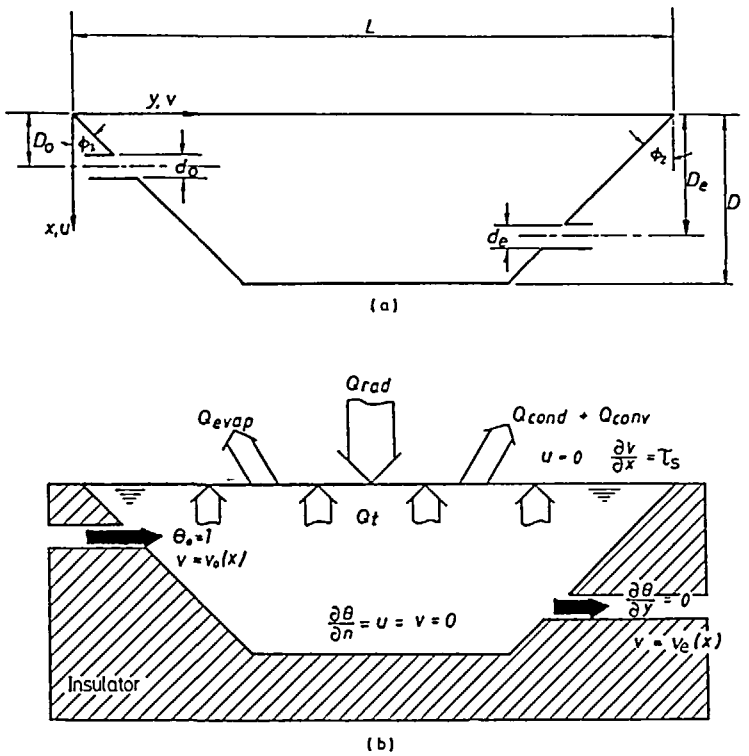

Figure 1 (a) Co-ordinate system of trapezoidal chamber; (b) cooling chamber and its boundary conditions

with the vorticity defined as:

$$\tilde{\zeta}^* = -\nabla^{*2}\tilde{\psi}^* \tag{3}$$

and the velocities given by:

$$\tilde{u}^* = \nabla^* \times \tilde{\psi}^* \tag{4}$$

For two-dimensional problem:

$$\nabla^* = A_1 \frac{\partial}{\partial x^*}\hat{i} + A_2 \frac{\partial}{\partial y^*}\hat{j} \tag{5}$$

[From here on, the * representing dimensionless variables and quantities are omitted for simplicity.]

The inlet Reynolds number $R_o = V_o d_o/\nu$; densimetric Froude number $F_o = V_o/[g d_o(\rho_{ref} - \rho_o)/\rho_o]^{1/2}$; Prandtl number $Pr = \nu/\alpha$ and aspect ratios $A_1 = (d_o/X)$ and $A_2 = (d_o/Y)$. The symbols ρ, g, ν and α denotes respectively the density, gravitational acceleration, kinematic viscosity and thermal diffusivity; T is the temperature of the fluid. Subscript 'o' indicates some reference state, say that of the inlet warm fluid. The coefficient β in the density–temperature relationship is taken as constant.

BOUNDARY CONDITIONS

Thermal boundary conditions

Rigid boundaries are assumed adiabatic, therefore $\partial\theta/\partial n = 0$, where n is the direction normal to the boundary. The temperature at the inlet is assumed to be uniform. At the outlet, heat is assumed transferred across this boundary by convection alone (i.e. $\partial\theta/\partial y = 0$). At the ambient-liquid interface (*Figure 1b*), heat is transferred to the atmosphere by radiation (Q_{rad}), evaporation (Q_{evap}) and by conduction (Q_{cond}) and convection (Q_{conv}). The thermal condition at the chamber liquid surface, due to the heat load introduced from the inlet to the chamber, is therefore given by $\partial\theta/\partial x = K\theta_s$ at $x = 0$. The value of K is primarily a function of the ambient air speed and the equilibrium (natural surface) temperature of the liquid body as defined by Edinger[4–6] and Jobson[15].

Velocity boundary conditions

Velocities for the rigid non-slip walls are $u = v = 0$. At the liquid reservoir surface, $u = 0$ and the effect of air movement over the surface is modelled by a non-deformable surface shape, with ψ at the surface = constant. The applied dimensionless wind stress due to air movement at the liquid surface $\tau_s = -\partial v/\partial x$ is assumed constant[23–25]. In the absence of air movement, $\tau_s = 0$. Velocities at the inlet and outlet region of the chamber reservoir are specified.

Stream function and vorticity boundary conditions

For solid non-slip wall ψ = constant and $\zeta = -A_n^2(\partial^2\psi/\partial n^2)$, where A_n is a non-dimensionalized directional constant. At the free surface, $u = 0$, ψ is a constant and $\zeta = A_1(\partial v/\partial x)$ = constant. Other boundary conditions for ψ and ζ must be derived from those for velocity in such a way that the solution obtained by using ψ and ζ are identical to that obtained by using u, v and p.

NUMERICAL SOLUTION PROCEDURES

Following Mallinson and de Vahl Davis[46] and Behnia *et al.*[47], in order to speed up the convergence rate to steady state solution of (1)–(2), the approach adopted here is to introduce false transient factors (α_ϕ) into the time derivative terms in (1)–(2), which allow relative changes to be made in the time rates of change of ϕ($\phi = \zeta$ or θ), i.e. to replace the time derivative terms

in (1)–(2) with $(1/\alpha_\phi)(\partial/\partial t)$. Further change is also made to replace (3) by the parabolic equation:

$$\frac{1}{\alpha_\psi}\frac{\partial \psi}{\partial t} = \nabla^2 \psi + \zeta \tag{6}$$

Numerical experiments show that, by using the above approach and with the proper choice of the α_ϕ values, steady state solution of (1)–(2) can be reached with considerably less computational effort than with the set of steady state elliptic equations.

Furthermore, in order to provide a simplified and accurate finite-difference treatment of the boundary conditions on non-rectangular boundaries, the physical region as show in *Figure 2a* is transformed into a rectangular domain (*Figure 2b*) by introducing new coordinates ξ and η, in which:

$$\begin{aligned} \xi &= ax \qquad && \text{for } 0 \leqslant x \leqslant D \\ \eta &= b\left[\frac{y - F_1(x)}{F_2(x) - F_1(x)}\right] L \qquad && \text{for } 0 \leqslant y \leqslant L \end{aligned} \tag{7}$$

where a, b are scaling factor, chosen such that $0 \leqslant \xi \leqslant 1$ for $0 \leqslant x \leqslant D$ and $0 \leqslant \eta \leqslant 1$ for $0 \leqslant y \leqslant 1$. Functions $F_1(x)$ and $F_2(x)$ describe the left-hand and right-hand boundary of the reservoir respectively. This transformation is generally satisfactory provided $F_2(x) - F_1(x) \neq 0$.

In the transformed ξ–η region, the equations in terms of ξ and η are:

$$\frac{1}{\alpha_\psi}\frac{\partial \psi}{\partial t} = B_1\frac{\partial^2 \psi}{\partial \xi^2} + B_2\frac{\partial^2 \psi}{\partial \xi\, \partial \eta} + B_3\frac{\partial^2 \psi}{\partial \eta^2} + B_4\frac{\partial \psi}{\partial \eta} + \zeta \tag{8}$$

with

$$u = E_3\frac{\partial \psi}{\partial \eta}; \qquad v = -\left(E_1\frac{\partial \psi}{\partial \xi} + E_2\frac{\partial \psi}{\partial \eta}\right) \tag{9}$$

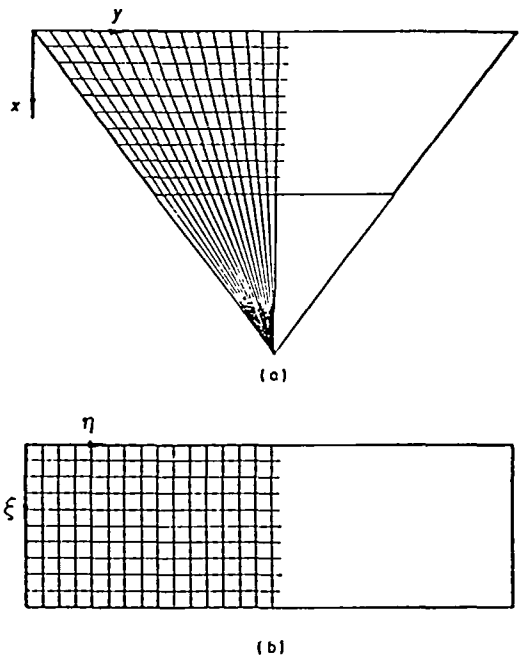

Figure 2 (a) Location of computational points in physical space; (b) transformed computational mesh

and the transport equations may be generalized as:

$$\frac{1}{\alpha_\phi}\frac{\partial\phi}{\partial t}+D_1\frac{\partial(u\phi)}{\partial\xi}D_2\frac{\partial(u\phi)}{\partial\eta}D_3\frac{\partial(v\phi)}{\partial\eta}=c\left[D_4\frac{\partial^2\phi}{\partial\xi^2}+D_5\frac{\partial^2\phi}{\partial\xi\,\partial\eta}+D_6\frac{\partial\phi}{\partial\eta}\right]+S_\phi \tag{10}$$

where ϕ stands for θ or ζ. The constant c is $(1/R_o)$ for the vorticity transport equation and $(1/R_oPr)$ for the energy transport equation. 'B's, 'D's and 'E's are spatial 'constants' resulting from the transformation. They are functions only of the positions in the ξ–η plane. These coefficients are required only to be computed once in each solution. S_ϕ are the source terms of the transport equations with $S_\theta=0.0$ for the energy transport equation and $S_\zeta=f(F_o,\theta,\xi,\eta)$ for the transport equation.

The finite-difference solution of (8)–(10) were obtained with the rectangular mesh system defined in *Figure 2b*. The numerical procedure used involves an alternating direction implicit (ADI) method originally proposed by Peaceman and Rachford[48] and modified by Samarskii and Andree[49]. For the governing transport equations, the advancement over one time step is accomplished through:

$$\begin{aligned}[I-\sigma\Delta tA_\xi](\phi)^*&=[A_\xi+A_\eta](\phi)^n+(S_\phi)^n\\ [I-\sigma\Delta tA_\xi](\phi)^{**}&=(\phi)^*\\ (\phi)^{n+1}&=(\phi)^n+\Delta t(\phi)^{**}\end{aligned} \tag{11}$$

where $(\phi)^*$ and $(\phi)^{**}$ are dummy variables; A_ξ and A_η are matrix operators formed through finite differencing of the governing equations in the ξ and η directions respectively; $(S_\phi)^n$ is the source term evaluated at the most recent solution field; σ is a weighted time-step factor; I is an identity matrix. This scheme is equivalent to:

$$\frac{(\phi)^{n+1}-(\phi)^n}{\Delta t}=(A_\xi+A_\eta)(1-\sigma)(\phi)^n+(A_\xi+A_\eta)\sigma(\phi)^{n+1}-\sigma^2(A_\xi A_\eta)[(\phi)^{n+1}-(\phi)^n]+(S_\phi)^n \tag{12}$$

For $\sigma=1/2$, the above scheme corresponds to the Crank–Nicholson equation.

In the above finite-difference formulations, all spatial derivatives are approximated by second-order-accurate centre differences. The convective terms in (10) are approximated by using a second order up-wind differencing method. The mixed spatial derivatives resulting from the mesh transformation are handled by the method proposed by McKee and Mitchell[50]. The resulting linear set of finite difference equations is then solved by an algorithm due to Thomas (see Roach[51]). Three-point backward and forward difference formulae are used for derivatives at the boundaries. Estimates of boundary values of vorticity and temperature are obtained after each iteration in the ADI procedure and are used as more up-to-date approximations in the second half of the ADI procedure. The source term of each equation is calculated using the latest field value available.

The boundary finite difference vorticity values are obtained by considering the Taylor series expansion of ψ into the solution region and taking into consideration the ψ and the velocity at the boundary, i.e. along the parallel walls:

$$\zeta_W=-\frac{3C_n}{(\Delta\xi)^2}(\psi_{W+1}-\psi_W)-\frac{1}{2}\zeta_{W+1} \tag{13}$$

and along the inclined walls:

$$\zeta_W=-\frac{3C_n}{(\Delta\eta)^2}(\psi_{W+1}-\psi_W)-\frac{1}{2}\zeta_{W+1} \tag{14}$$

where C_n and C'_n are spatial constants resulting from transformation. Subscripts $W+1$ and W refer to the wall and the adjacent internal mesh point value respectively.

It was initially hoped that the bulk of the results could be obtained using a 51×101 mesh, and that this mesh would be fine enough to show, with reasonable accuracy, the general features of the flow. At low Reynolds number and high densimetric Froude number, the solutions obtained were qualitatively acceptable. However, at high Reynolds number ($R_o > 500$) and low densimetric Froude number ($F_o < 1$), truncation errors were large and unrealistic temperature fields resulted. A finer mesh of 101×201 was then used, and a marked improvement occurred in all the solutions. Further refinement in the mesh size produced little changes in the result. This degree of consistency was deemed acceptable here to use the 101×201 mesh in view of the very large increase in computer cost required to obtain the minor benefits of any further increases in accuracy. Hence, unless otherwise specified, a 101×201 mesh was used in all the solutions described here.

For the numerical time step (Δt) selection, it was found that a suitable Δt can be chosen empirically by examining the source term of the governing equation. If the source term of a governing equation is relatively small compared with the convection term and/or diffusion term (e.g. the ζ–ψ equation), or if the source term is zero (e.g. the θ-equation), then the Δt can be chosen according to the Courant–Friedrich–Lewy condition[51], i.e. the upper limit on the Δt was determined by:

$$\alpha_\phi \Delta t \leqslant \frac{\Delta x}{|u_{max}|} \quad \text{and} \quad \alpha_\phi \Delta t \leqslant \frac{\Delta y}{|v_{max}|} \tag{15}$$

whichever was the smaller. If the source term of the governing equation is very large, then the Δt for these equations is governed by a parameter λ, given by:

$$\alpha_\phi \Delta t \leqslant \lambda \Big/ \left[2\left(\frac{1}{\Delta x^2} + \frac{1}{\Delta x^2} \right) \right] \tag{16}$$

where $1 \leqslant \lambda \leqslant 2$. The source term of the ζ transport equation lies between those described for conditions (15) and (16). If the $F_o \gg 1$, then the source term of the ζ-equation is relatively small. The motion is governed predominantly by the initial momentum of the jet. Condition (15) may then be used for the selection of time step. However, if $F_o \leqslant 1$, then buoyancy may dominate the motion. The source term in the ζ-equation is relatively large and condition (16) is used for the time step selection.

RESULTS AND DISCUSSION

In a study of this nature, it is inevitable that a large amount of results on computer output has been accumulated. It is obviously impossible to present all of these results here. In the discussions that follow, relatively few actual numerical results are presented and emphasis is placed upon what is, in a sense, the broader view of the problem, namely the analysis of the trends or expected behaviour rather than particular results.

When fluid is drawn from a chamber, heated by some processes and discharged back to the chamber to dissipate its heat load to the ambient, an orderly fluid motion can be observed within the cooling chamber. This fluid motion and subsequent heat transfer from the surface of the cooling chamber is governed by the condition of discharge, the shape and size of the chamber. Since fluid under normal condition has a positive coefficient of thermal expansion, the warm fluid tends to rise to the surface and spread. This occurs because regardless of the reduction of buoyancy by mixing, the warm inflow is always buoyant with respect to the ambient fluid. Thus, if the heated fluid is discharged below the surface of the cooling chamber, it will tend to rise and remain afloat over the ambient fluid as a stratified layer. For the opened cooling chamber, the exposure of the upper surface of the incoming heated fluid to the atmosphere results in a larger temperature excess near the surface and thus allows greater temperature reduction by surface heat loss. If the heated surface fluid is discharged into the cooling chamber in such a

way that minimum mixing occurs between the heated effluent and the receiving body of fluid, then heat dissipation to the atmosphere is at the highest rate since the surface-layer temperature is at a maximum.

The two main dimensionless parameters used in studying the cooling chamber problem (in which the inertia forces, buoyancy forces and viscous forces control the phenomenon) are the densimetric Froude number F_o and the Reynolds number R_o. The following numerical experiments illustrate the role of F_o and R_o in establishing the flow pattern.

Variation of F_o has a significant effect on the trajectories of the buoyant inflow. *Figures 3* and *4* show the effects of variation of F_o (with $R_o=500$) on the streamline and isotherm contours for the cooling chamber numerical experiments. These Figures show that the incoming heated fluid spread from a buoyant plume-like discharge for $F_o=0.5$ and 1.0 to a less buoyant jet-like discharge for $F_o=2.5$ and $F_o=50$. The depth of the submerged inlet is at $D_o/d_o=1.5$ below the fluid surface. In these Figures and others that follow, unless noted otherwise, the contour lines $1,2,\ldots,9$ represent the contour level of 10%, 20%,...,90% of $(\phi_{max}-\phi_{min})$, where $\phi=\psi$ for *the streamline contours and* $\phi=\theta$ *for the isotherm contours. It should be noted that all the* results are plotted at a 'reduced scaling', Hence, for reservoirs with wall-slopes of 45° and $L/D=10$ say, the horizontal length is substantially compressed and the apparent wall-slopes are not 45°.

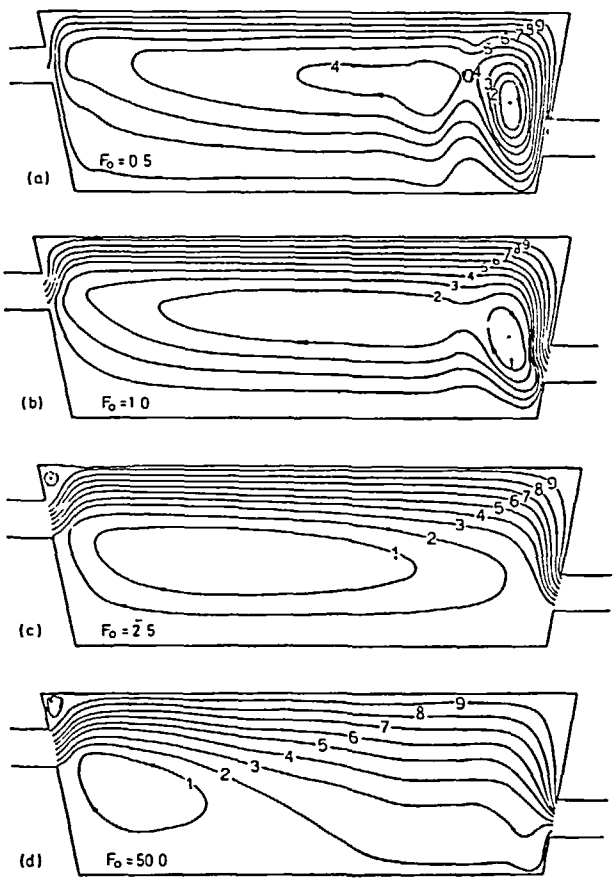

Figure 3 Effects of densimetric Froude number (F_o) on streamlines. $R_o=500$, $L/D=10$, $D/d_o=5$, Wall Slopes=45°. (a) $F_o=0.5$; (b) $F_o=1.0$; (c) $F_o=2.5$; (d) $F_o=50.0$

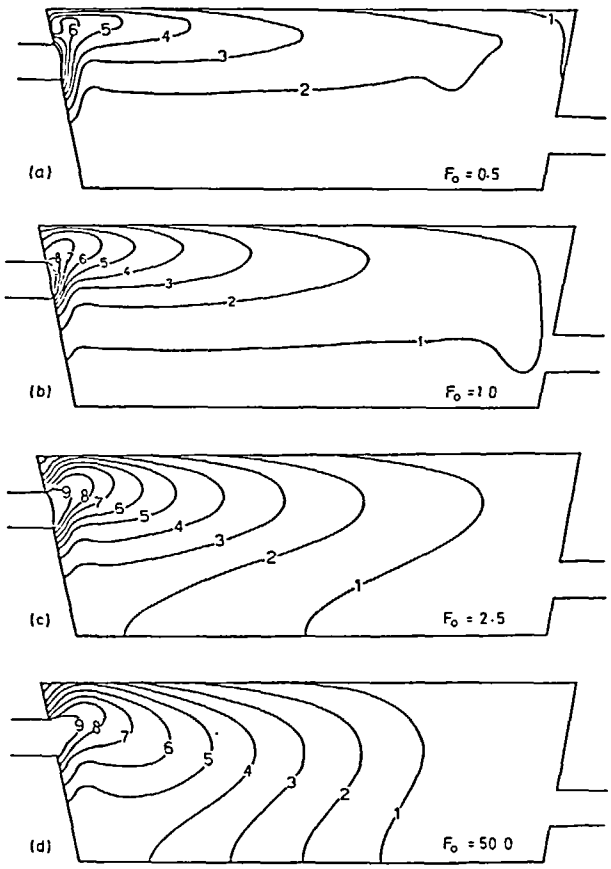

Figure 4 Effects of densimetric Froude number (F_o) on isotherms. $R_o=500$, $L/D=10$, $D/d_o=5$, Wall Slopes=45°. (a) $F_o=0.5$; (b) $F_o=1.0$; (c) $F_o=2.5$; (d) $F_o=50.0$

For $F_o=0.5$ and $R_o=500$, (*Figure 3a* and *Figure 4a*), the numerical experiment shows a very buoyant inflow to the chamber. There is an almost immediate rise of the trajectory of the warm fluid as it enters the reservoir. The warm fluid then spreads towards the surface and remains afloat near the surface region until it reaches the downstream boundary. Here, the fluid is being forced down the end wall and the ambient temperature is also relatively large. Some secondary and tertiary motions as described by de Vahl Davis and Mallinson[33] in a natural convection problem, were observed to form near the outlet region. These motions consist of two strong secondary eddies, and a very weak tertiary eddy in between the two larger secondary eddies. The effects of these secondary and tertiary eddies are shown in the distortion of the 20% isotherm in *Figure 4a*. Further study of the isotherms in *Figure 4a* indicates the predominant effects of buoyancy. Warmer fluid and larger temperature gradients exist in the upper half of the chamber, with most of the lower half being isothermal.

As F_o is increased to 1.0 at $R_o=500$, the secondary eddies near the outlet region combine to form a single eddy. The eddy centre is located near the outlet region. Distortion of the isotherms can now be seen in *Figure 4b* for the 10% contour line. Here, the buoyant force of the incoming heated fluid is of the same order of magnitude as its inertia force. The warm fluid thus rises immediately as it enters the basin, but not as sharply as when $F_o=0.5$ When the warm fluid reaches the surface, it still possesses sufficient buoyancy and horizontal momentum to cause it

to spread out as a narrow warm layer across the chamber. As a result, larger horizontal velocity always occurs at the free surface. As the surface current reaches the downstream wall, it is being forced down to the outlet. This results in large downward velocity near the downstream wall. Furthermore, the viscous driving force origination from this downward movement of the fluid near the end wall causes a circulation eddy to form near the outlet region. The streamline contour further shows that cold entrainment fluid is being brought from the deeper region to the warm inlet region. This causes appreciable velocities near the bottom of the chamber in the opposite direction to the velocities near the surface. Experimental results obtained by Pleasance[44] show similar circulation patterns for a similar problem.

As F_o is further increased, the circulation and surface flow pattern change dramatically. The eddy centres in *Figure 3a* ($F_o=0.5$, $R_o=500$) and *Figure 3b* ($F_o=1.0$, $R_o=500$) have shifted to the middle of the reservoir as F_o is increased to 2.5 (*Figure 3c*). If F_o is further increased to 25, the eddy centre moves nearer to the inlet region (*Figure 3d*).

Further studies of the isotherm and streamline contours of the cooling chamber through numerical experiments show the gradual spreading of the incoming flow towards the bottom of the reservoir as F_o is increased. This is particularly evident in the solution with $F_o=25$ which represents a solution for relatively cool non-buoyant inflow (*Figure 3d* and *Figure 4d*). The inertia force of the incoming heated fluid here is very much greater than the buoyant force. Hence, incoming fluid did not have sufficient buoyancy to rise and spread towards the surface immediately as it enters the chamber. Instead, the fluid rises very gradually as it enters the chamber, but diffuses quickly over the entire chamber's depth at a small distance away from the inlet. As a result, the surface current is not as high as those described for $F_o=1.0$. Moreover, the outlet fluid in this case is drawn from a wide region of the chamber (*Figure 3d*). The downward current near the outlet region is thus also not as large. With $F_o=25$, numerical experiments also indicate that the clockwise circulation region has greatly reduced in size and is confined nearer to the inlet region. A small circulation is also observed just above the inlet region, entraining into the incoming heated fluid from above. The temperature distribution away from the inlet region is found to be fairly uniform.

Numerical experiments with varying R_o for constant F_o are shown in *Figures 5* and *6* (with F_o held constant at 1.0). For large R_o, the heated fluid has sufficient horizontal momentum and buoyancy to cause the heated fluid to spread out near the surface region across the chamber. At low R_o the isotherms appear to form a diffusion like pattern near the inlet region (with F_o held constant, the initial rate of rise of the trajectory of the warm fluid is the same for all the Raynolds numbers considered). It should, however, be cautioned here that as R_o varies at constant F_o, the values of (T_o-T_{ref}) can be different for different sets of numerical experiments without being evident in the solutions. For example, as R_o increased, V_o in the definition of $R_o=V_o/v_o$ increases for fixed d_o and v_o. For F_o to remain constant with increasing V_o, implies that $\Delta\rho_o$ in the definition $F_o=V_o/\sqrt{[(\Delta\rho_o/\rho_o)gd_o]}$ has to increase proportionally. Thus, an increase in R_o with F_o held constant could also mean $\Delta T_o=(T_o-T_{ref})$ has increased implicitly. Hence, the behaviour of the fluid in the reservoir away from the inlet region with increasing R_o exhibits much similar behaviour to that of decreasing F_o values.

In *Figure 7*, the vertical temperature profiles for varying F_o and R_o are plotted for each case of $F_o=0.5$, $F_o=2.5$, $F_o=25$ (with R_o fixed at 500); and $R_o=250$, $R_o=500$, $R_o=1000$ (with F_o fixed at 1.0). The symbols B, C,...,H represent the vertical temperature profile at positions with $\eta=1/8$, 1/4, 3/8, 1/2, 5/8, 3/4, 7/8 respectively. As F_o increase, the warm-fluid layer spreads from a stratified type of flow ($F_o=0.5$) to a more diffusive type of flow ($F_o=25$). The main feature of the transition is the gradual disappearance of the warm-surface layer as F_o is increased and the fluid reaches the downstream boundary at a lower mean excess temperature concentration. As F_o decreases, a higher level of the excess temperature concentration reaches the downstream boundary.

Figure 7 also shows that, with F_o fixed at 1.0, increases in Reynolds number results in transferring more excess heat to the downstream boundary. However, for the same F_o, the flow patterns near the inlet region are always similar. Away from the inlet region, R_o then determines

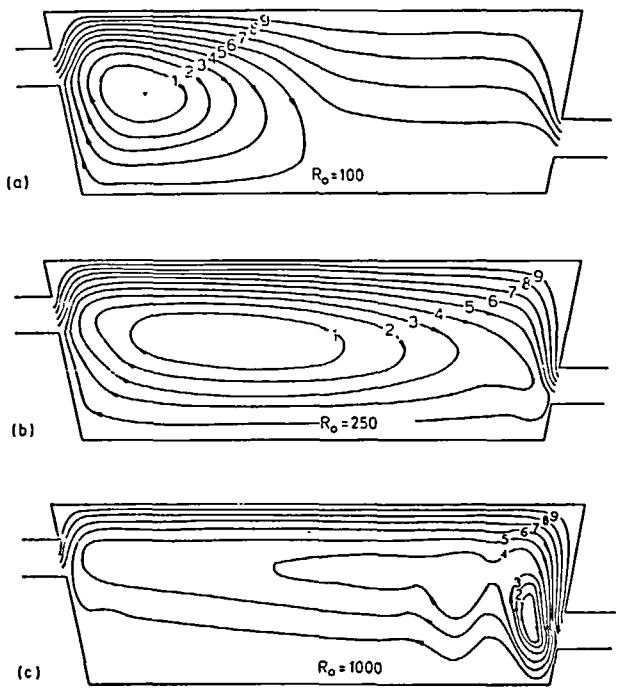

Figure 5 Effects of inlet Reynolds number (R_o) on streamlines. $F_o=1.0$, $L/D=10$, $D/d_o=5$, Wall Slopes=45°. (a) $R_o=100$; (b) $R_o=250$; (c) $R_o=1000$

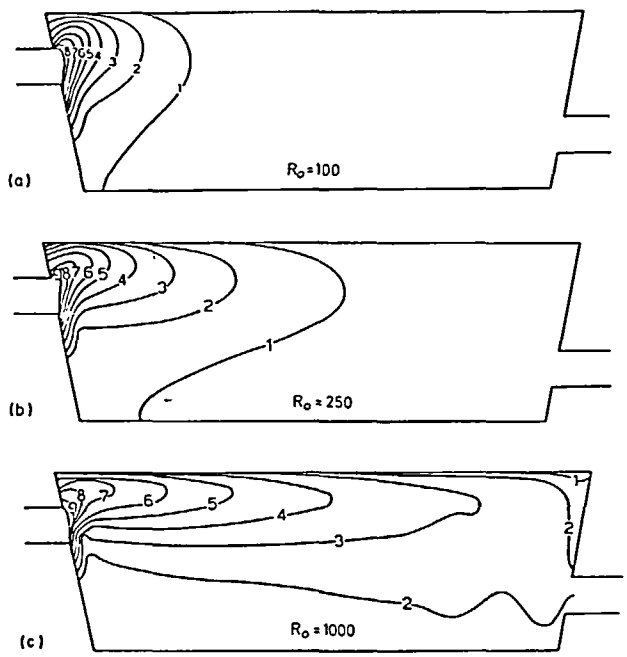

Figure 6 Effects of inlet Reynolds number (R_o) on isotherms. $F_o=1.0$, $L/D=10$, $D/d_o=5$, Wall Slopes=45°. (a) $R_o=100$; (b) $R_o=250$; (c) $R_o=1000$

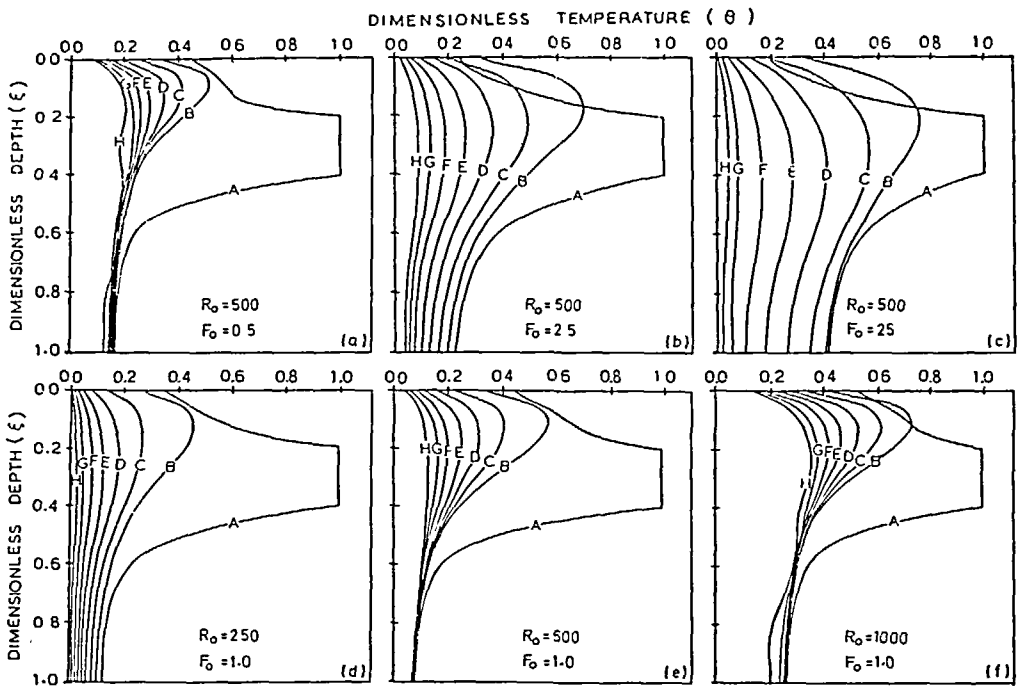

Figure 7 Vertical temperature profiles. (a) $R_o=500$, $F_o=0.5$; (b) $R_o=500$, $F_o=2.5$; (c) $R_o=500$, $F_o=25.0$; (d) $F_o=1.0$; $R_o=250$; (e) $F_o=1.0$; $R_o=500$; (f) $F_o=1.0$; $R_o=1000$. [A:$\eta=0$, B:$\eta=1/8$, C:$\eta=1/4$, D:$\eta=3/8$, E:$\eta=1/2$, F:$\eta=5/8$, G:$\eta=3/4$, H:$\eta=7/8$]

whether the flow still possess sufficient horizontal momentum to spread the fluid out near the surface or let the fluid diffuse throughout the fluid body.

Further study of *Figure 7* shows that the temperature profiles are vertical at the floor, indicating that the adiabatic wall condition is well satisfied. Heat transfer processes are also evidenced from these vertical temperature profiles. Along the surface, the temperature distributions show that there is always a vertical temperature gradient near the surface region at steady state. This phenomena develops for steady state solution when there is heat transfer across the surface of the liquid.

The local value of the vertical temperature gradient along the liquid surface of the chamber is also a measure of the local heat transfer rate. It varies along the surface and generally decreases in the direction of the motion. Along the surface, heat is lost to the surrounding atmosphere; and the surface, temperature (and subsequently the temperature in the chamber reservoir) decreases away from the inlet region. As a result, the local temperature difference between the surface and the surroundings decreases, and the local heat transfer rate also decrease. In general, the cooler region in the chamber reservoir away from the inlet region tends to catch up with the warm inlet region. Thus, as the heated liquid moves downstream, the temperature profiles also show a flattening effect, indicating decreasing in vertical heat transfer. The vertical temperature profiles are also strongly affected by the general circulation pattern in the chamber. Near the surface region, the profiles show that convection and diffusion heat transfer processes are significant. This temperature pattern is due to the spreading motion generated by the strong surface current and the horizontal momentum of the incoming jet. Along the bottom of the chamber, the profiles are more conduction-like, because the velocities in this region are relatively small compared with the surface current.

Typical cooling chamber reservoir velocity profiles are represented in *Figure 8* with the numerical experiments for $F_o=2.5$, $R_o=500$. *Figure 8a* indicates that, except near the two end

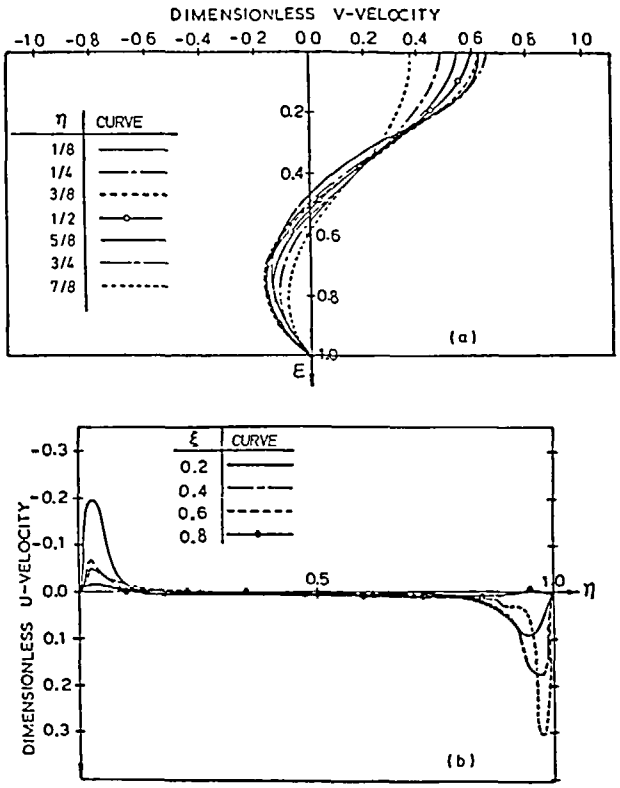

Figure 8 Typical dimensionless u- and v-velocity profiles. $L/D=10$, $D/d_o=5$, Wall Slopes$=45°$, $F_o=2.5$, $R_o=500$

walls, the surface current is usually in the positive η-direction, and a reverse current in the interior returns the mass flux. The depth dividing the forward and return current varies significantly with locations. The depth generally increases with increasing distance away from the inlet region. The corresponding vertical u-velocity distributions for various constant depth of ξ are displayed in *Figure 8b*. It indicates down-welling in the downstream half of the reservoir and up-welling in the upstream half of the reservoir. The vertical velocities are larger near the inlet and outlet wall regions of the reservoir. The reason for this is the inclination of the walls at these locations. Above the inlet region, the buoyancy of the warm fluid forces the flow upwards; below the inlet region, colder return fluid flows up to replace fluid entrained into the inflowing warm fluid. Near the outlet region of the reservoir, surface flow is being forced downwards towards the outlet region. In the middle of the reservoir, the flow is mostly horizontal i.e. $u \approx 0$.

Besides the predominant effects of F_o and R_o on the cooling chamber fluid flow and heat transfer characteristics, the inlet dimension relative to the dimensions of the reservoir, and the topography of the reservoir are also important factors in influencing the cooling chamber solutions. The cooling chamber into which heated fluid is injected may be shallow relative to the dimension of the inlet opening. Examples of this occur for some power station cooling ponds because the near-shore areas adjacent to the power plant sites are often shallow and because large quantities of heated water discharged usually require discharge ducts of large dimensions. The flow pattern of the buoyant discharges in shallow reservoir is thus influenced by the interaction of the jet with the bottom and with free surface. On the other hand, if the reservoir is deep, the heated fluid may not reach the bottom of the reservoir. For a large (long) reservoir, the heated fluid will almost certainly be cooled to ambient temperature before it reaches the

downstream region. However, if the reservoir is small (short), the heated fluid may remain warm when it reaches the downstream region.

Comparison between *Figure 9* with *Figure 3c* and *Figure 4c* shows the changes in the flow and temperature patterns as the relative dimensions of the depth and inlet of the reservoir given by the ratio (D/d_o) is varied from 5 to 10. For the particular numerical experiments considered here, the parameters held constant are $F_o = 2.5$, $R_o = 500$, $L/D = 10$ and wall-slopes = 45°. For $D/d_o = 5$, the heated fluid has spread to the bottom of the relatively 'shallow reservoir'. For $D/d_o = 10$, there is sufficient buoyancy to keep the heated fluid afloat as a stratified layer, and the reservoir is deep enough (relative to the inlet dimension) to prevent the heated fluid reaching the bottom. For $D/d_o = 5$, some of the heated fluid has spread to the bottom.

Varying the length to depth ratio (L/D) of the reservoir also produces changes in the flow and temperature patterns in the cooling reservoir solutions. *Figure 10*, in comparison with *Figure 3b*

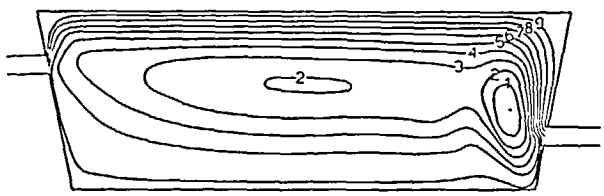

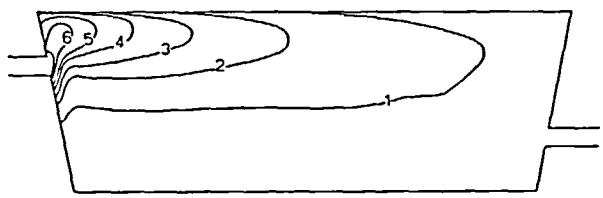

Figure 9 Effects of D/d_o on cooling chamber heat and fluid flow. $D/d_o = 10$, $R_o = 500$, $F_o = 2.5$, $L/D = 10$, Wall Slopes = 45°

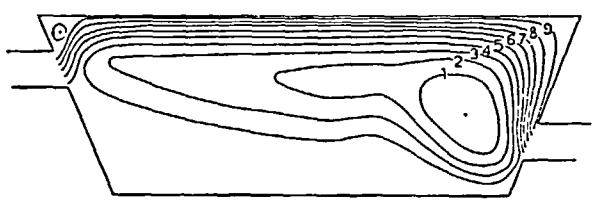

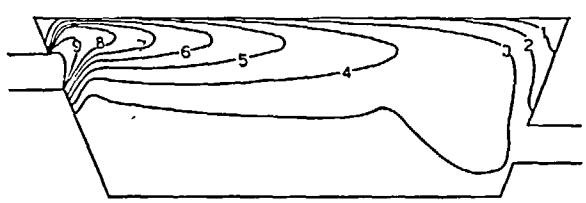

Figure 10 Effects of L/D on cooling chamber heat and fluid flow. $L/D = 5$, $R_o = 500$, $F_o = 1.0$, $L/d_o = 5$, Wall Slopes = 45°

and *Figure 4b*, shows that for lower values of L/D (say, $L/D=5$ with other parameters held constant), the heated fluid may not have sufficient surface area to dissipate its heat load to the atmosphere before reaching the outlet region.

Varying the depth of submergence of the inlet and the slope of the reservoir also significantly affects the flow pattern in the reservoir; especially near the inlet and outlet regions (compare *Figure 11* with *Figure 3a* and *Figure 4a*). Since most fluid has a positive coefficient of thermal expansion, incoming heated fluid tends to rise and float near the surface of the receiving fluid. With submerged inlet, the effect on the heated fluid trajectory is the deflection of the jet upward in the vertical direction as the heated fluid enters the reservoir. Submerged discharges into the reservoir are also characterized by high dilution. The greater the submergence of the inlet below the fluid surface, the larger the temperature reduction at the surface. If the heated fluid is discharged into the reservoir at the surface, then the temperature reduction and mixing is minimal; and the heat transfer at the surface is larger than for submerged discharge into the reservoir.

If the heated liquid is introduced into the reservoir in such a way that minimum mixing occurs between the heated effluent and the receiving body of cooling fluid, then heat dissipation to the atmosphere is at the highest rate since the surface-layer temperature is at a maximum. In many instances, however, maximum-temperature criteria prevent use of this method since the temperature of the fluid surface layer may be above permissible value.

COMPARISON WITH FINDINGS OF OTHER INVESTIGATORS

Numerical models, while based on theoretical equations that represent the physical processes, are only approximations to the real physical processes involved. As a result, experimental evidence and field data are required to establish the accuracy and applicability of the numerical model. Experimental work on buoyant jets are many[11,14,16,24–26]. However, experiments suitable for direct comparison with the numerical results obtained here were few. One of these available for comparison was done by Pleasance[44]. The dimensionless parameters considered in the experiments were in the range of $F_o=0.70$ to 4.5 and $R_o=180$ to 1200 for a rectangular cooling chamber. The results of the experiments and the corresponding numerical solutions are presented in *Figures 11* and *12*. The experimental results exhibit a strong forward current in a narrow layer near the surface with much smaller velocities beneath this layer as indicated in *Figure 11a*. A reverse current occurs somewhere near the bottom of the reservoir to return the mass flux entrained into the surface layer near the inlet region. This behaviour is consistent with what was obtained in the numerical experiments with vertical walls as indicated in the same *Figure 11a*. There is some indication that, due to the influence of the physical side walls in the experiments and the two-dimensional constraint imposed on the numerical model, the strength of the reverse flow in the laboratory simulation of the problem was not as great as that predicted by the numerical model. Further study of the centreline temperature decay pattern away from the inlet region is shown in *Figure 12*. It shows that the profile of temperature decay away from the inlet region obtained from the numerical experiments followed closely to those observed in the experiments. Studies of temperature distributions on prototype cooling reservoirs were also made by many workers[3,8–13,17]. Their results vary considerably from site to site. However, in general, these indicate large temperature gradients and significant vertical convection near the inlet to the cooling reservoir. One such vertical temperature profile obtained by Summers *et al.*[26] at a site near an inlet to the cooling pond is shown in *Figure 11b* with some numerically obtained vertical temperature profiles near the inlet to the cooling chamber. It can be seen that the dimensionless vertical temperature distribution near the inlet region of a prototype cooling reservoir is similar to those obtained by the numerical experiments.

In the present numerical experiments, the flow field in the cooling chamber is sensitive to the value of F_o. The thickness of the heated liquid layer very clearly increases as the F_o was increased. These phenomena were also observed in the experiments conducted by Tamai *et al.*[27] and Hayashi and Shuto[11]. Their experiments were performed for a warm water jet discharged horizontally at the surface of a body of deep water. The dimensionless parameters considered

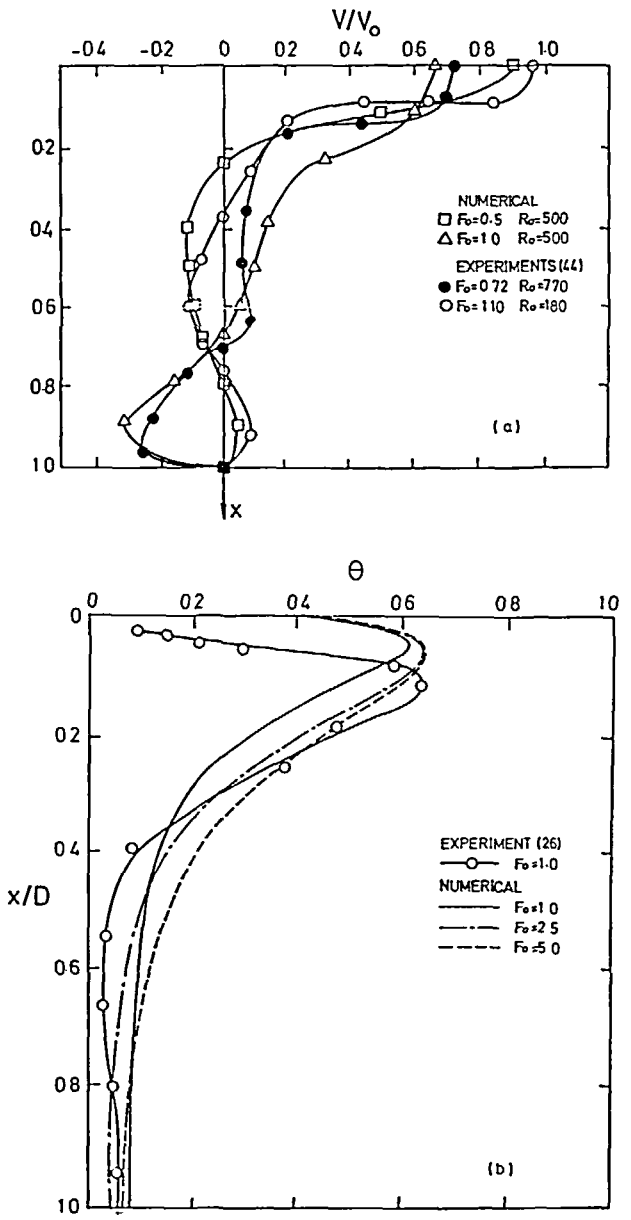

Figure 11 Comparison with experimental and field measurements with numerical experiments. (a) Vertical velocity profiles; (b) vertical temperature profiles

by Tamai *et al.* are of F_o ranged from 2.4 to 11.3 and R_o ranged from 6.6×10^3 to 2.1×10^4. Those described by Hayashi and Shuto are of $F_o=1.4$ to 16.1 and $R_o=5.6\times10^3$ to 3.1×10^4. Tamai *et al.* and Hayashi *et al.* observed that for small values of $F_o\leqslant2.6$ a narrow stream of warm water formed along the surface, with very little mixing or spreading. The smaller the F_o, the thinner the surface layer of heated water. These phenomena were also observed in the present numerical experiments as shown in *Figures 3* and *4*.

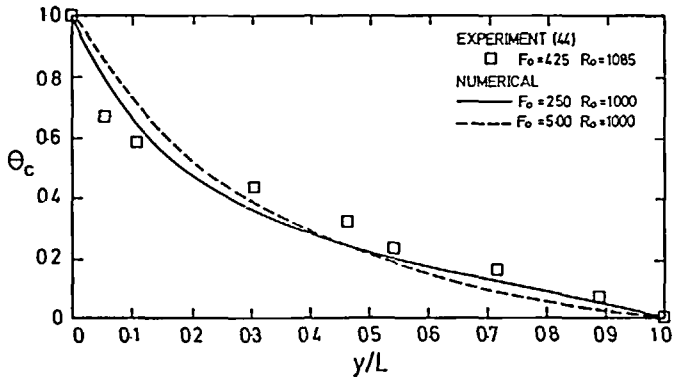

Figure 12 Comparison of observed temperature decay profiles with numerical experiments

In another study, Stefan[23,24] and Stefan and Schiebe[25] presented laboratory results for heated jets entering a basin. The inlet jet dimensions in the study were much smaller than the basin depths. Vertical isotherm plots were presented along the jet centreline for F_o of 0.62 and 0.72. These plots indicate large temperature gradients and significant vertical convection near the inlet wall, and a stratified warm layer formed near the surface away from the inlet region. This behaviour is similar to that shown for the present numerical experiments for small F_o (*Figures 3a–b* and *Figures 4a–b*). Their temperature gradients were larger than the numerical results obtained here. This is believed to be due to the two-dimensional constraint imposed on the present numerical model which does not take into account the lateral spreading of the buoyant fluid and thus results in too much diffusion in the vertical direction. However, in general, their vertical isotherms are very similar to those obtained by the present numerical experiments. They also presented some velocity plots which exhibited a strong current in a narrow layer near the surface with much smaller velocities beneath this layer and some of the velocities near the bottom are in the opposite direction to those of the surface currents. The present numerical experiments also exhibit similar behaviour.

Comparison with the numerical solutions obtained by other investigators is difficult as similar numerical solutions are not available. The velocity vector solutions obtained by Roberts and Streets[19] for heated water discharged into a simulated 'sloping-dam' provided some features for comparison. Their results show the development of the flow over time. The R_o of the flow is about 100 and the F_o is estimated to be around 0.4. Hence, the heated water is highly buoyant and as it enters the 'dam', it spreads out, rises to the surface almost immediately and, moves across the 'dam' in a surface current. The density current is then forced down to the outflow and circulation pattern begin to form in response to the entrainment of fluid. The driving by the viscous forces originating from the surface layer flow and the downward movement of the fluid near the outlet region, further enhanced the circulation. These phenomena are also observed in the present numerical experiments for small F_o as shown in *Figure 3a* and *Figure 4a* for similar trapezoidal cooling chamber.

CONCLUSIONS

The flow fields and temperature profiles in a flow-through trapezoidal cooling chamber are strong function of both the F_o and R_o. Variation of F_o has a significant effect on the trajectories of the buoyant inflow. Numerical experiment shows that for small F_o, there is an almost immediate rise of the trajectory of the warm fluid as it enters the chamber. The warm fluid then spreads towards the surface and remains afloat near the surface region until it reaches the downstream boundary. As F_o is increased, the circulation and surface flow pattern change dramatically. The

isotherm and streamline contours of the cooling chamber show the gradual spreading of the incoming flow towards the bottom of the reservoir as F_o is increased. The behaviour for the increase in R_o (with fixed F_o) is qualitatively similar to that for a decrease of F_o with R_o held constant. For the opened trapezoidal cooling chamber considered here, the submergence ratio D/d_o, chamber length to depth ratio L/D and chamber wall angles are also significant in influencing the flow fields.

ACKNOWLEDGEMENTS

The author gratefully acknowledges the financial support of a National University of Singapore Research Grant (No. RP33/84) and the assistance of W. M. Ong and S. J. Yap during the course of this project.

REFERENCES

1 Barry, R. E. and Hoffman, D. P. Computer model for thermal pollution, *J. Power Div., ASCE*, **93** (PO1), 117–132 (1972)
2 Boericke, R. R. and Hall, D. W. Hydraulics and thermal dispersion in an irregular estuary, *J. Hydr. Div., ASCE*, **100**, 85–102 (1974)
3 Coulter, C. G., Guthrie, A., Kirkwood, J. B., Lamb., A. N. and Watson, K. S. Thermal discharge from power stations, *Conf. Thermal Discharge: Eng. Ecol., Sydney*, Inst. Engrs, Australia, pp. 37–45 (1972)
4 Edinger, J. E. and Geyer, J. C. *Heat Exchange in the Environment*. Edison Electric Institute Publication No. 65-902 (1965)
5 Edinger, J. E., Euttweiler, D. W. and Geyer, J. C. The response of water temperature to meteorological conditions, *Water Resour. Res.*, **4**, 1136–1142 (1968)
6 Edinger, J. E. and Geyer, J. C. Analyzing steam electric power plant discharges, *J. Sanit. Eng. Div., ASCE*, **94** (SA4), 611–622 (1968)
7 Farrow, D. E. Convective circulation in reservoir sidearms of small aspect ratio. *Proc. Tenth Austr. Fluid Mech. Conf., Melbourne*, pp. 15.41–15.43 (1989)
8 Harbeck, G. E. The use of reservoirs and lakes for the dissipation of heat, *U.S. Geol. Survey Circ. 282* (1953)
9 Harbeck, G. E., Koberg, G. E. and Hughes, G. H. The effect of the addition of heat from a power plant on the thermal structure and evaporation of Lake Colorado City, Texas, *Prof. paper 272-B*, U.S. Geological Survey (1959)
10 Harleman, D. R. F. and Stolzenbach, K. D. Fluid mechanics of heat disposal from power generation. *A. Rev. Fluid Mech.*, **4**, 7–32 (1972)
11 Hayashi, T. and Shuto, N. Diffusion of warm water jets discharged horizontally at the water surface, *Proc. 12th Congr. Int. Ass. Hydr. Res., Fort Collins*, **4**, 47–59 (1967)
12 Hayashi, T., Shuto, N. and Kawakami, K. Basic study on the diffusion of warm water jets discharged from power plants into bays, *Coastal Eng. in Jaoan*, Vol. 10, Japan Soc. of Civil Engrs., pp. 129–142 (1967)
13 Hindley, P. D., Miner, R. M. and Cayot, R. Thermal discharge: a model-prototype comparison, *J. Power Div., ASCE*, **97** (PO4), 783–798 (1971)
14 Jen, Y., Wiegel, R. L. and Mobarek, I. Surface discharge of horizontal warm-water jet, *J. Power Div., ASCE*, **92** (PO2), 1–30 (1966)
15 Jobson, H. E. The dissipation of excess heat from water systems, *J. Power Div., ASCE*, **99** (PO4), 89–103 (1973)
16 Koh, R. C. Y. Two-dimensional surface warm jets, *J. Hydr. Div., ASCE*, **97**, 819–836 (1971)
17 Parker, F. L. and Krenkel, P. A. Physical and engineering aspects of thermal pollution. Thermal pollution: Status of the art; *Report No. 3*, Department of Environmental and Water Resources, Vanderbilt Univ. (1969)
18 Paul, J. F. and Lick, W. J. A numerical model for a three-dimensional, variable-density jet, *Report No. FTAS/TR-7B-92*, Div. of Fluid. Thermal and Aerospace Sciences, Case Inst. Technol. (1974)
19 Roberts, B. R. and Street, R. L. Two-dimensional, hydrostatic simulation of thermally-influenced hydrodynamics flows, *Tech. Rept. No. 194*, Civil Engineering Dept., Stanford Univ. (1975)
20 Sengupta, S. and Lick, W. J. A numerical model for wind driven circulation and temperature fields in lakes and ponds, *Report No. FTAS/TR-74-99*, Div. Fluid, Thermal and Aerospace Sciences, Case Inst. Technol. (1974)
21 Snider, D. M. and Viskanta, R. Thermal stratification by radiation in surface layers of stagnant water, *Thermophys. Heat Transfer Conf.*, Boston, MA, *ASME paper No. 74-HT-44* (1974)
22 Spraggs, L. D. and Street, R. L. Three-dimensional simulation of thermally-influenced hydrodynamic flows, *Tech. Rep. No. 190*, Civil Engineering Dept., Stanford Univ. (1975)
23 Stefan, H. Modelling spread of heat water over lake, *J. Power Div., ASCE*, **96** (PO3), 469–482 (1979)
24 Stefan, H. Three-dimensional jet-type surface plumes in theory and in the laboratory, *Project Report No. 126*, St. Anthony Falls Hydraulic Lab., Univ. of Minnesota, Minneapolis (1971)
25 Stefan, H. and Schiebe, F. R. Experimental study of warm water flow into impounds, Part III. Temperature and velocity fields near a surface outlet in three-dimensional flow, *Project Report No. 103*, St. Anthony Falls Hydraulic Lab., Univ. of Minnesota, Minneapolis (1968)

26 Summers, W. R., Ellyett, C. D. and Kennewell, J. Infra-red scanning techniques applied to quantitative analysis of thermal plumes, *Conf. Thermal Discharge: Eng. Ecol. Sydney*, Inst. of Engrs, Australia, pp. 46–51 (1972)
27 Tamai, N., Wiegel, R. L. and Tornberg, G. F. Horizontal surface discharge of warm water jets, *J. Power Div., ASCE*, **95** (PO2), 253–276 (1969)
28 Bejan, A. and Tien, C. L. Laminar natural convection heat transfer in a horizontal cavity with different end temperatures, *ASME J. Heat Transfer*, **100**, 641–647 (1978)
29 Catton, I. Natural convection in enclosures, *Proc. 6th Int. Heat Transfer Conf., Toronto*, Vol. 6, Hemisphere Press, Washington, DC, pp. 13–31 (1978)
30 Chen, K. S., Ho, J. R. and Humphrey, J. A. C. Steady, two-dimensional, natural convection in rectangular enclosures with differently heated walls, *ASME J. Heat Transfer*, **109**, 400–406 (1987)
31 Chung, K. C. and Trefethen, L. M. Natural convection in vertical stack of inclined parallelogrammic cavities, *Int. J. Heat Mass Transfer*, **25**, 277–284 (1985)
32 Davalath, J. and Bayazitoglu, Y. Forced convection cooling across rectangular blocks, *ASME J. Heat Transfer*, **109**, 321–328 (1987)
33 de Vahl Davis, G. and Mallinson, G. D. A note on natural convection in a vertical slot, *J. Fluid Mech.*, **72**, (Part I), 87–93 (1975)
34 Iyican, L., Bayazitoglu, Y. and Witte, L. C. An analytical study of natural convective heat transfer within a trapezoidal enclosure, *ASME J. Heat Transfer*, **102**, 640–647 (1980)
35 Iyican, L., Witte, L. C. and Bayazitoglu, Y. An experimental study of natural convection in trapezoidal enclosures, *ASME J. Heat Transfer*, **102**, 648–653 (1980)
36 Lam, S. W., Gani, R. and Symons, J. G. Natural convection in trapezoidal cavities, *3rd Austr. Conf. Heat Mass Transfer, Melbourne*, pp. 87–94 (1985)
37 Lee, T. S. Computational and experimental studies of convective fluid motion and heat transfer in inclined non-rectangular enclosures, *Int. J. Heat Fluid Flow*, **5**, 29–36 (1984)
38 Nielson, P. V. Flow in air conditioned rooms, *PhD Thesis*, Danfoss A/S, Nordborg, Denmark (1974)
39 Oberkampf, W. L. and Crow, L. I. Numerical study of the velocity and temperature fields in a flow through reservoir. *ASME J. Heat Transfer*, **98**, 353–359 (1976)
40 Ozoe, H., Mouri, A., Ohmuro, M., Churchill, S. W. and Lior, N. Numerical calculations of laminar and turbulent natural convection in water in rectangular channels heated and cooled isothermally on the opposing walls, *Int. J. Heat Mass Transfer*, **28**, 125–138 (1985)
41 Ozoe, H., Mouri, A., Hiramitsu, M., Churchill, S. W. and Lior, N. Numerical calculation of the three-dimensional turbulent natural convection in a cubical enclosure using a two-equation model for turbulence, *ASME J. Heat Transfer*, **108**, 806–813 (1986)
42 Patankar, S. V. Recent developments in computational heat transfer, *ASME J. Heat Transfer*, **110** (4B), 1037–1045 (1988)
43 Patterson, J. C. Unsteady natural convection in a cavity with internal heating and cooling, *J. Fluid Mech.*, **140**, 135–140 (1984)
44 Pleasance, G. E. Heat transfer in stratified flow, *MEng Thesis*, School of Civil Engineering, University of New South Wales, Sydney (1974)
45 Poulikakos, D. and Bejan, A. The fluid mechanics of an attic space, *J. Fluid Mech.*, **131**, 251–269 (1983)
46 Mallinson, G. D. and de Vahl Davis, G. The method of false transient for the solution of coupled elliptic equations. *J. Comp. Phys.*, **12**, 435–461 (1973)
47 Behnia, M., Wolfstein, M. and de Vahl Davis, G. A stable fast marching scheme for computational fluid mechanics, *Int. J. Num. Meth. Fluids*, **10**, 607–621 (1990)
48 Peaceman, D. W. and Rachford, H. H. Jr. The numerical solution of parabolic and elliptic differential equations, *J. SIAM*, **3**, 23–41 (1955)
49 Samarski, A. A. and Andree, V. B. On a highly accuracy difference scheme for an elliptic equation with several space variables. *USSR Comp. Math. Phys.*, **3**, 1373–1382 (1983)
50 Mckee, S. and Mitchell, A. R. Alternating direction methods for parabolic equations in two space dimensions with a mixed derivative. *The Computer J.*, **13** (1), 81–86 (1969)
51 Roach, P. J. *Computational Fluid Dynamics* Hermosa, Albuquerque, NM (1972)
52 Courant, R., Friedrichs, K. and Lewy, H. On partial difference equations of mathematical physics, *IBM J. Res.*, pp. 215–234 (1967)